Star detection and tracking algorithm of autoguiding

Cai Wenjuan, Wang Liqiang, Yuan Bo

(State Key Laboratory of Modern Optical Instrumentation, CNERC for Optical Instrumentation, Zhejiang University, Hangzhou 310027, China)

Abstract: The basic principle of autoguiding was introduced in detail, which included the proper star selection and tracking algorithm. Considering that the star energy distribution in the image was approximately Gaussian distribution, a reliable target star selection method was proposed. The algorithm analyzed a threshold value of the image firstly, and then a number of candidate stars were detected according to the threshold condition. The target star was selected from the candidate stars by guiding criterion. Finally, the centroid coordinate of the target star was calculated through Gaussian fitting. The accuracy of the target star detection and calculating speed were both improved, the experimental results showed that the proposed algorithm can achieve a good autoguiding performance.

Key words: star tracking; star selection; autoguiding

CLC number: TP311; TP316 Document code: A Article ID: 1007-2276(2014)08-2684-06

自动导星星点检测及跟踪算法研究

蔡文娟,王立强,袁 波

(浙江大学 现代光学仪器国家重点实验室,国家光学仪器工程技术研究中心,浙江 杭州 310027)

摘 要:详细介绍了自动导星的工作原理,对自动导星的星点检测及跟踪算法进行研究,结合星点能量在星图上分布近似高斯分布的特性,提出一种稳定可靠的目标星点提取算法。算法首先分析了星点目标的阈值判断原则,根据阈值条件确定一定数量的候选星点,然后在候选星点中筛选出最优的目标星点,最后通过高斯曲线拟合的办法求取最优目标星点的质心坐标。该方法提高了目标星点提取的准确性和计算速度,实验结果表明:改进后的算法能够达到良好的效果。

关键词:星点追踪; 星点检测; 自动导星

收稿日期:2013-12-21; **修订日期**:2014-01-24

基金项目:国家科技攻关计划基金(2012BAI14B06,2011BAI12B06);中央高校基本科研业务专项基金(2013FZA5018)

作者简介:蔡文娟(1989-),女,硕士生,主要从事数字图像处理方面的研究。Email:caiwenjuan@zju.edu.cn

导师简介:王立强(1976-),男,副教授,博士,要从事光机电一体化仪器方面的研究。Email:wangliqiang@zju.edu.cn

0 Introduction

In the deep sky astrophotography, in order to offset the phenomenon of the movement of stars caused by the Earth's rotation and eliminate stars cable resulting from enough exposure time, equatorial is used to drive the telescope to move in the opposite direction of the Earth's rotation so that the real-time tracking of stars can come true. The method can achieve a good result at the same time. However, the equatorial rotation rate is not exactly the same as the Earth, because of its production and installation errors[1].

The equatorial cannot correct errors mentioned by itself. In order to improve the tracking precision, two cameras are often used in tracking photography, a main camera and a tracking camera. The tracking camera can view the brightest star on account of its characteristics, including short exposure time, short telescope's focal length, small relative aperture and a large field of view. Tracking the brightest star in the relatively large field of view can compensate the gap quickly, which makes a good result in deep sky photography.

Specific approach is as follow: Firstly, the star images are captured by CCD fixed behind the guider. Then the computer will deal with the real-time images. When the shift of tracked target star is detected, the offset will be calculated and transmitted to the equatorial as feedback. Then the equatorial will correct the tracking error, to achieve the goal of real-time tracking. In autoguiding algorithm, target star point extraction and centroid location are the key steps. The recognition accuracy of target star and the precision of centroid coordinate calculation directly affect the final equatorial tracking accuracy.

In the traditional star detection process, all the stars in the image are detected. This method is a waste of time. To improve the calculating speed, combined with the practical application of autoguider, a new target star point detection algorithm is proposed, which considers the brightness, size and position of the stars in the image.

1 Introduction of autoguiding procedure

Autoguider works through real-time detection of the position of the target star to achieve the star tracking. As shown in Fig.1, under the conditions of long exposure, CCD transfers the captured star image to a computer, the computer automatically selects the optimal picture as the tracking target star, and then calculates the target star centroid coordinate, compared with that of the same star in the initial picture. If offset occurs, the computer sends the offset to equatorial to drive the lens to rotate corresponding to the offset. So real-time tracking is achieved.

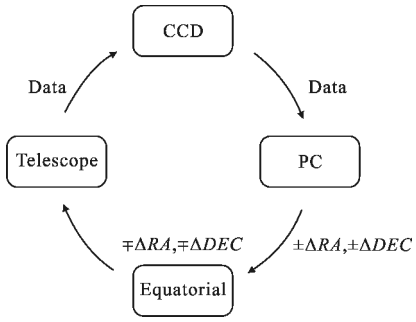

Fig.1 Flow chart of automatic guide

Assuming that the tracking target star is in a coordinate axis composed of RA and DEC, and the centroid coordinate of the tracking target star in initial image is $(\mathbf{RA}_0, \mathbf{DEC}_0)$, so in the equatorial track target star process, the real-time coordinate of the target star can be expressed as$(\mathbf{RA}_0 \pm \Delta\mathbf{RA}, \mathbf{DEC}_0 \pm \Delta\mathbf{DEC})$, ± represent the directions of the offset respectively, $\Delta\mathbf{RA}$ and $\Delta\mathbf{DEC}$ represent offset. If $\Delta\mathbf{RA}$ and $\Delta\mathbf{DEC}$ are not equal to zero, the offset and direction will be transmitted to a computer, then the computer sends the offset to the equatorial to make it move to the opposite direction. Therefore, the equatorial can correct the tracking errors.

2 Extraction and positioning of target star

The detection of star is the key step of auto

guider system. Generally, star detection is mainly divided into two parts: star detection and centroid localization. The common star detection techniques are mainly connected component labeling method, gray cross projection[2-3] and so on. Star centroid extracted is mainly based on two factors, grayscale and edge. The edge-based method mainly includes edge circle fitting, Hough transform, etc., this method is suitable for large target. Grayscale-based method includes centroid, surface fitting etc., this method is more suitable for small and gray uniform target. Star targets are generally small, more suitable for the method based on grayscale.

The traditional star detection algorithm always executes threshold segmentation before detection. Allowing for that deep sky pictures taken with less noise, a high contrast ratio between background and target star area, in order to reduce the algorithm step and improve the detection rate, this paper adopts the dynamic box search method[4] to directly detect the star on the star image after filtering processing without binarization.

2.1 Star detection

In the traditional star detection process, all the stars in the image are detected. Combined with the practical application of auto guider, it only needs to find one star as the tracking target, which is called optimal star.

In order to extract the optimal star quickly and accurately, a certain number of brighter stars are selected as candidates. In deep sky astrophotography, the darkest magnitude that human eyes can differentiate is generally the sixth magnitude, which is an area of greater than or equal to 3×3 pixels in the star image. Firstly the stars that meet the above conditions are selected as candidates, and then the optimal star can be found among the candidates.

2.1.1 Star energy distribution characteristics

Star point can be seen as a point light source at infinity, so the image on the photosensitive surface of the image sensor can be regarded as a point-like spot in dark background .This energy distribution of the point-like spot approximate Gaussian distribution[5], so the star center is the energy peak[6]. For the brighter star point, its average value is much higher than noise average value, while for dark star point, its energy value is close to or smaller than the noise point energy value, so it is difficult to calculate the centroid coordinates accurately. These stars are not generally treated as the target stars.

2.1.2 Threshold determination

The threshold of star detection means effectively distinguishing star from the background and filtering out noise, and it is useful to identify the target star. The principal contributors to the background signal noise are typically: read noise, inhomogeneity of the dark current, and the dark current noise itself. It is possible to estimate the background noise as the standard deviation of all pixel values in a dark frame[7]. In consideration of the background noise, location of the target star in the real star image are constantly changing, gray average value and standard deviation of the image are considered as a threshold reference factors, an adaptive threshold selection method is chosen as the star point detection standards, the expression is:

$$V_{th}=E+k\delta \tag{1}$$

Where E is the mean value of the pixels; δ is the standard deviation of the pixel values; k is a weighting coefficient, usually associated with the image noise, desirable 3-5[8].

2.1.3 Star detection algorithm

The dynamic search box can achieve the star extraction. However, this algorithm is more suitable for single-star detection, while for multi-star detection it is complex. In this paper, drawing on the basis of the above algorithm, an algorithm more suitable for detecting target star under multi-star condition is proposed.

The energy distribution of star is similar to Gaussian distribution, so finding the grayscale peak of star area is equiva lent to detecting the energy

distribution of the center point. Firstly finding the energy center,, and then taking that point as the center and connecting the outside by square window, Dynamic search box is shown in Fig.2.

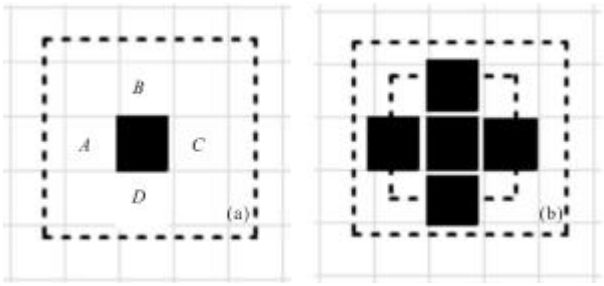

Fig.2 Schematic diagram of Dynamic search box

Taking 3×3 window for example, calculating the average gray value of **A**,**B**,**C**,**D** in the window, if the value is greater than the threshold, this area is considered belong to the target area, and then expanding the scope of the window until you find the area that doesn't meet the condition, and finally recording the center coordinates and window size of the region. The window whose effective area is smaller than 3×3 is considered as noise area. At the same time,the overexposure condition may result in bright spot which will affect the selection of the optimal star, so the area larger than the size of 15×15 is considered as a noise point, which will be removed. Finally the center coordinates and window size of the star that meet the condition are saved as candidates tothe final target star extracted.

2.2 Detection and centroid localization of target star

After the above steps, some interference noise points are exclued, so it is possible to quickly extract the target star.

2.2.1 Detection of target star

Generally, the star with bigger area, higher brightness and closer to the central field of view is detected as optimal. The part of 2.1 has already detected the candidate star group and saved the center coordinates and window sizes. In the process of extracting the optimal star, considering the regional average energy and size of the region, whether it is closer to the center of the field of view and some other factors, an optimal star point criteria is presented:

$$\mathbf{T}=k_1\mathbf{R}_1+k_2\mathbf{E}+k_3/\mathbf{R}_2 \quad (2)$$

Where $\mathbf{R}_1$ represents the radius of the star area, $\mathbf{E}$ is the average grayscale value of the star point area, k_1, k_2, k_3 respectively stand for the weighting coefficient. $k_1=0.3$, $k_2=0.3$, $k_3=0.4$. $\mathbf{R}_2$ is the distance between the target star center and the center of the field of view.

2.2.2 Centroid coordinate calculation

Because the star energy distribution is similar to Gaussian distribution, the traditional centroid algorithm could not obtain high accuracy. Gaussian fitting method can achieve a better result in calculating centroid coordinate.

Based on **n** a point light source law which is generally symmetrical two-dimensional Gaussian distribution, Gaussian fitting extracts the coordinates of the center point of the target star. Imaging feature of point light source is highest pixel gray value in the center, the nearer to the edge the smaller. So Gaussian surface fitting can fit the digitized target star, and then determine the target star gray center position.

Gaussian fitting equation can be expressed as:

$$f(\mathbf{x},\mathbf{y})=\mathbf{A}\times\exp\{-\frac{1}{2(1-\rho^2)}[\left(\frac{\mathbf{x}-\mathbf{x}_0}{\sigma_x}\right)^2- 2\rho\left(\frac{\mathbf{x}}{\sigma_x}\right)\left(\frac{\mathbf{y}}{\sigma_y}\right)+\left(\frac{\mathbf{y}-\mathbf{y}_0}{\sigma_y}\right)^2]\} \quad (3)$$

A represents the maximum of Gaussian surface that is related to the level of star, the higher level, the brighter it is. $(\mathbf{x}_0,\mathbf{y}_0)$ is the center of Gaussian function, σ_x and σ_y are the standard deviation of x-axis and y-axis; ρ is a correlation coefficient. To simplify calculation, often let $\rho=0$, $\sigma_x=\sigma_y=\mathbf{B}$, So the equation can be expressed as:

$$f(\mathbf{x},\mathbf{y})=\mathbf{A}\times\exp\left(\frac{-\mathbf{r}^2}{\mathbf{B}}\right) \quad (4)$$

B stands for the size of the light spot, $\mathbf{r}^2=(\mathbf{x}-\mathbf{x}_0)^2+(\mathbf{y}-\mathbf{y}_0)^2$, $\mathbf{x}_0$ and $\mathbf{y}_0$ are the coordinates of star centroid.

Gaussian surface fitting makes use of the Gaussian distribution of the star grayscale value, so

the accuracy of the target star centroid is relatively high, but computational complexity increases a lot, To simplify the algorithm and improve calculating rate, only **x** and **y** directions are respectively Gaussian curve fit.

The star extracting process has already get the maximum points of star area (x_p,y_p), which has completed the star point centroid coarse positioning in fact [9]. Additionally this step had already saved the size of star region. So it can make Gaussian curve fitting.

The pixel grayscale distribution equation can be expressed as:

$$g_{ij}=A_1\times\exp\left(-\frac{(x_i-x_p-\Delta x)^2}{B_1}\right) \tag{5}$$

$$g_{ij}=A_2\times\exp\left(-\frac{(y_i-y_p-\Delta y)^2}{B_2}\right) \tag{6}$$

Δx and Δy are the coordinate deviations of centroid, ($x_p+\Delta x$,$y_p+\Delta y$) is the centroid coordinate after Gaussian fitting.

3 Realization of autoguiding

Firstly, the target star is selected from the image that CCD captured, and then its centroid coordinate is calculated, this will be regarded as the original reference. The new centroid coordinate of the target star in the image captured later is also calculated. These two centroid coordinates are used to get the offset position of the target star. The offset values are the tracking error of equatorial and are transmitted to the computer equatorial for tracking error correction and real-time tracking.

4 Experimental results

As shown in Fig.3 and Fig.4, the candidate star group is obtained through detection of the star image, then the optimal star can be find through the candidate star group, finally by Gaussian fitting respectively in the **x**-direction and **y**-direction, so Gaussian curve fitting can be got, thus the desired coordinates of the centroid of the star can be obtained.

Fig.3 Original star image

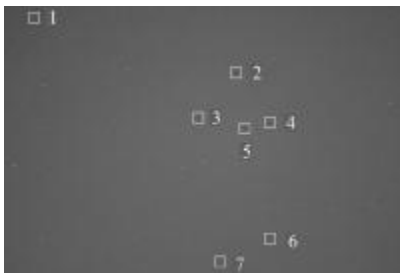

Fig.4 Detected star point

The **T** value of the marked star found is shown in Tab.1.

Tab.1 T values of candidate stars

Star	1	2	3	4	5	6	7
T	329	1 122	376	374	352	355	448

It follows that the largest value of **T** of candidate stars is the second one. So the second star is chosen as the target star.

As shown in Fig.5 and Fig.6, the result shows that

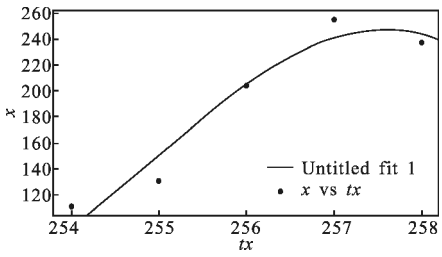

Fig.5 **x**-direction Gaussian fitting

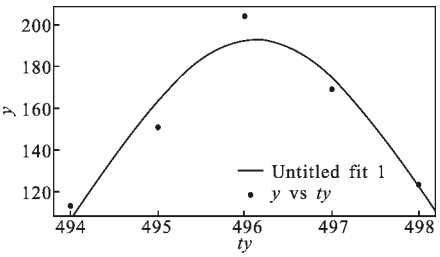

Fig.6 **y**-direction Gaussian fitting

the crude target star coordinates is (496,256), while calculated through Gaussian fitting centroid, the final coordinates is(496, 258).

This method will remove noise ponits, including brighter but small ponits. In addition, it will make the equatorial always track the optimal star, which has a relatively larger average gray value, bigger area and more closer to the center of the field of view.

5 Concluions

The algorithm proposed in this paper firstly finds the candidate star group, then extracts the target star search process, it simplifies the calculation process compared with the traditional star point tracking algorithms. In the target star discovery process the goal is clearer. However, based on Gaussian fitting, the centroid algorithm is still complicated and computationally intensive; the rate of the algorithm has yet to be further improved.

Reference:

[1] Li Hui, Yan Huimin, Wang Ligiang. A high accuracy automatic star tracking system based on embedded platform [J]. Optical Instruments, 2009, 31(4): 70-73. (in Chinese)

[2] Xu Wei. Star fast extraction and high accuracy centroid estimation of star camera [D]. Hangzhou: Zhejiang University, 2013. (in Chinese)

[3] Chen Zheng. The research of star image locating and identifying technology [D]. Xi'an: Xidian University, 2010.

[4] Tao Yulu, Deng Xinpu, Cheng Hongwei. Research on star acquisition method based on dynamic box [J]. Aerospace Electronic Warfare, 2012, 28(5): 34-37. (in Chinese)

[5] Wei Wei, Liu Enhai. Preprocessing of infrared star map and position accuracy analysis of star point [J]. Infrared and Laser Engineering, 2014, 43(3): 992-996. (in Chinese)

[6] Li Xuekui, Tan Huishu, Zhang Huanming, et al. Guide star identification method for star sensor [J]. Computer Engineering and Application, 2010, 46(21): 220-222. (in Chinese)

[7] Liebe C C. Accuracy performance of star trackers-a tutorial [J]. Transactions on Aerospace and Electronic Systems IEEE, 2002, 38(2): 587-599.

[8] Liao Yufu, Zhong Jianyong. A new method used for star distillation of near-infrared star image of star tracker [J]. Infrared and Laser Engineering, 2014, 43(5): 1668-1671. (in Chinese)

[9] Wang Haiyong, Fei Zhenghong, Wang Xinlong. Precise simulation of star spots and centroid calculation based on Caussian distribution [J]. Optical and Precision Engineering, 2009, 17(7): 1673-1676. (in Chinese)

小尺寸光斑中心的高精度定位算法

赵婧鑫,周富强

(北京航空航天大学 仪器科学与光电工程学院,北京 100191)

摘　要:光斑中心定位是光学测量中的关键技术之一,针对小尺寸光斑中心定位算法精度低等问题,提出了一种具有高精度的小尺寸光斑中心两步定位算法。通过寻找一阶导数零交叉点的方法确定光斑中心所在的像素级坐标,然后利用该中心邻域内不饱和点的灰度信息进行高斯拟合计算光斑中心亚像素级坐标。实验结果表明:在无噪声污染光斑图像中,与其他经典算法相比,两步定位算法误差远小于 0.05 像素,保证了光斑中心的高精度定位,且光斑成像越接近理想高斯分布,精度越高。

关键词:小尺寸光斑; 中心定位; 零交叉; 高斯拟合

中图分类号:TP391.4　　**文献标志码**:A　　**文章编号**:1007-2276(2014)08-2690-04

High-precision center location algorithm of small-scale focal spot

Zhao Jingxin, Zhou Fuqiang

(Institute of Instrument and Opto-Electronics Engineering, Beihang University, Beijing 100191, China)

Abstract: Spot center location is a key technique in the field of optical measurement. A Two-step method for center location of small-scale focal spot with high precision was proposed to solve the problem as the low precision when using classic center location algorithms. First, the pixel-level center could be located through zero crossing of the first derivative in the focal spot image. And then, the unsaturated part of the focal spot beside the pixel-level center was used to fit the Gaussian surface to calculate the sub-pixel center. Experimental results show that, when comparing with other classic center location algorithms, the error of the two-step method is much less than 0.05 pixels in the spot image without background noise. The two-step method can keep high-precision center location of the focal spot. If the imaging model of the focal spot is much more similar with the ideal Gaussian spread function, the precision is higher.

Key words: small-scale focal spot; center location; zero-crossing; Gaussian fitting method

收稿日期:2013-12-10; **修订日期**:2014-01-25

基金项目:国家自然科学基金(61372177)

作者简介:赵婧鑫(1987-),女,硕士生,主要从事图像处理与识别方面的研究工作。Email:jingxinde@gmail.com

导师简介:周富强(1972-),男,教授,博士生导师,主要从事计算机视觉、图像处理与识别、三维数字化技术和激光及光电测试技术方面的研究工作。Email:zfq@buaa.edu.cn

0 引 言

光斑图像[1]是现有图像处理中较为常见的图像,光斑质心是光斑图像的重要特征之一。快速精确定位成像光斑的中心,是卫星导航、视觉测量等领域诸多应用的基础,对系统整体性能有着重要的影响。

点状光斑的中心定位方法可分为基于灰度和基于边缘的两大类[2]。基于灰度的方法一般利用目标的灰度分布信息,适用于半径较小且灰度分布均匀的光斑;基于边缘的方法一般利用目标的边缘形状信息,适用于半径较大的光斑。因此,小尺寸光斑通常采用基于灰度的方法进行中心定位。目前常用的基于灰度的中心定位方法包括三种:即质心法、Hessian 矩阵法和高斯拟合法。质心法[3]是用的最多的一种细分定位方法,它实现比较简单,运算速度快,而且有一定的定 位精度,但抗噪声能力弱,在实际应用中,通常对其进行改进,采用带阈值的质心法,可以获得更高的精度,抗噪声能力稍强于质心法。Hessian 矩阵可以用于判断曲线或曲面的局部极小值或极大值。Steger[4]利用 Hessian 矩阵得到图像中光条纹的法线方向,然后求法线方向上的极值点得到光条纹中心线的亚像素位置;魏振忠[5]在此基础上推导出光斑图像像素中心的 Hessian 矩阵判定条件,再利用二阶泰勒展开式推出亚像素中心的计算公式,该方法精度高,鲁棒性好,但要对整幅图像做大规模高斯卷积,运算量较大,且抗噪声能力不强。高斯拟合法精度较高,传统做法是利用质心法或二值化方法确定光斑区域,再根据高斯分布函数结合最小二乘法或插值法计算出光斑的中心坐标,方法复杂,速度慢,不适用于实时性较高的系统[6-8]。

针对上述方法的优势和不足,提出了一种高精度的小尺寸光斑中心两步定位算法。首先,通过寻找一阶导数零交叉点的方式准确定位小尺寸光斑像素级中心,再利用像素中心邻域内不饱和点的灰度信息进行高斯拟合计算小尺寸光斑的亚像素级中心坐标。实验结果表明,两步定位算法具有较高的精度。

1 像素级光斑中心定位

理论上,小尺寸光斑成像应聚集在一个像元内,但是单个像素的定位精度无法满足测量的要求,因此常采用散焦的方法,使光斑成像扩散到多个像素,再利用中心定位算法得到亚像素级的定位精度。小尺寸光斑目标图像的灰度分布为光学系统的点扩展函数,可以用二维高斯分布函数来近似表示:

$$g(x,y)=\frac{A}{2\pi\sigma^2}\exp\left(-\frac{(x-X)^2+(y-Y)^2}{2\sigma^2}\right)=B\times g(x)\times g(y) \quad (1)$$

式中:A 为小尺寸光斑像点的总能量;(X,Y)为函数中心点位置坐标;σ 是高斯函数的方差,对应光斑弥散半径的大小;$g(x)$和 $g(x)$分别为 x 和 y 方向的一维高斯分布函数。提取光斑中心实质上是求解公式(1)所示的二元函数的极大值点坐标。由公式(1)可看出高斯函数具有可分离性,因此对二元函数极大值点(X,Y)的求解可转化为,求解二维高斯函数每一行 x 方向一元函数像素极值点集合 $U(x_i,y_j)$和光斑图像每一列 y 方向一元函数像素极值点集合 $U(x_m,y_n)$,二者的交集即为二维高斯函数极值点(X,Y),即$(X,Y)=U(x_i,y_j)\cap U(X,y_n)$。图 1(a)所示为理想光斑的能量分布图,以 x 方向为例,图 1(b)所示为理想光斑 x 方向的能量分布函数曲线,其一阶导数分布曲线如图1(c)所示,可以看出,若点 X 为极大值点,则点 X 处的一阶导数为 0,且一阶导数在该点 X 邻域内递减。

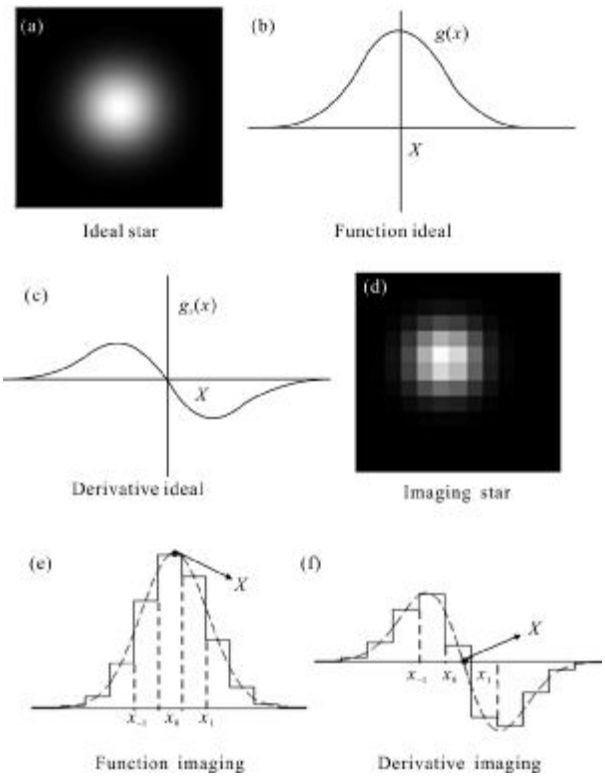

图 1 光斑成像模型

Fig.1 Imaging model of the spot

图 1(d)所示为实际获得的光斑图像,其灰度值分布是离散的,由此求出的图像一阶导数也是离散的,如图 1(e)所示,而图 1(f)所示的点 x_0 处一阶导数不为零,故无法简单地通过寻找一阶导数为零点来准确定位光斑的极大值点坐标。因此算法将光斑中心定位分为两个过程:(1) 首先定位小尺寸光斑的像素级中心点坐标(X_0,Y_0)。(2) 在点(X_0,Y_0)邻域内确定光斑的亚像素级中心坐标(X,Y)。

如图 1(e)和(f)所示,对三个连续的像素点 x_{-1}、x_0 和 x_1 进行分析,可看出若光斑中心 X 落在点 x_0 坐标内,则点 x_0 为光斑像素级中心点坐标,其一阶导数值 $g_x(x_0)$的绝对值在三点中最小,即$|g_x(x_0)|<|g_x(x_{-1})|$,且$|g_x(x_0)|<|g_x(x_1)|$,又由于点 x_0 为一阶导数过零点,即 $g_x(x_{-1})>0$,且 $g_x(x_1)<0$。同理若 y 方向上的像素点 y_0 为像素级中心点,则点 y_0 处的一阶导数值 $g_y(y_0)$的绝对值在其邻域内最小,且 $g_y(y_{-1})>0$,$g_y(y_1)<0$,则可推导出像素级光斑中心判定公式,即若在点(x_0,y_0)处,在 x 方向上,$|g_x(x_0)|<|g_x(x_{-1})|$,$|g_x(x_0)|<|g_x(x_1)|$,且 $g_x(x_{-1})>0$,$g_x(x_1)<0$,在 y 方向上,$|g_y(y_0)|<|g_y(y_{-1})|$,$|g_y(y_0)|<|g_y(y_1)|$,且 $g_y(y_{-1})>0$,$g_y(y_1)<0$,则点(x_0,y_0)即为光斑的像素级中心点坐标,记为(X_0,Y_0)。

2 亚像素级光斑中心计算

由第一节一阶导数零交叉法准确定位光斑图像像素级中心位置(X_0,Y_0)后,即可在该像素临域内确定光斑亚像素中心坐标(X,Y)。

由于光斑能量分布满足高斯分布函数,对公式(1)等式两边求对数,可得到:

$$\ln(g(x,y))=\ln(B)-\frac{(x-X)^2}{2\sigma^2}-\frac{(y-Y)^2}{2\sigma^2} \tag{2}$$

由于高斯函数具有可分离性,可在点(X_0,Y_0)处分别在 x 和 y 方向对光斑图像进行高斯拟合处理。以 x 方向为例,令 $\ln(C)=\ln(B)-(y-Y)^2/2\sigma^2$,将公式(2)转化为公式(3),则等式中包含 C、X 和 σ 三个未知数。

$$\ln(g(x,y))=\ln(C)-\frac{(x-X)^2}{2\sigma^2} \tag{3}$$

由公式(3)可知,光斑图像 x 方向上纵坐标相同的点所对应的 C 值是相同的。利用 CCD 采集光斑图像时,由于图像采集卡的有效位数通常为 8 位,当光强比较大或者 CCD 曝光时间过长时,容易导致数据饱和(灰度值超过 255),不能够反映出光斑的真实光强,如果把这些点也用于高斯拟合,则容易产生较大的误差,因此在进行高斯拟合的时候需要剔除这些饱和点[9]。而光斑半径较小,有效点也较少,因此可利用 x 方向上从属于同一光斑的三个像素点的灰度值构成方程组求解 X。假设三个点的横坐标为 x_1、x_2 和 x_3,对应的灰度值为 $g(x_1)$、$g(x_2)$和 $g(x_3)$,则可得到:

$$\begin{cases}\ln(g(x_1))=\ln(C)-\dfrac{(x_1-X)^2}{2\sigma^2}\\ \ln(g(x_2))=\ln(C)-\dfrac{(x_2-X)^2}{2\sigma^2}\\ \ln(g(x_3))=\ln(C)-\dfrac{(x_3-X)^2}{2\sigma^2}\end{cases} \tag{4}$$

同理,在点(X_0,Y_0)的 y 方向上取从属于同一光斑的三个像素点 3 个点 y_1、y_2 和 y_3 也可构成与公式(4)相似的方程组,则 X 和 Y 的求解公式为:

$$\begin{cases}X=\dfrac{1}{2}\cdot\dfrac{(x_3^2-x_2^2)\ln(g(x_1))+(x_1^2-x_3^2)\ln(g(x_2))+(x_2^2-x_1^2)\ln(g(x_3))}{(x_3-x_2)\ln(g(x_1))+(x_1-x_3)\ln(g(x_2))+(x_2-x_1)\ln(g(x_3))}\\ Y=\dfrac{1}{2}\cdot\dfrac{(y_3^2-y_2^2)\ln(g(y_1))+(y_1^2-y_3^2)\ln(g(y_2))+(y_2^2-y_1^2)\ln(g(y_3))}{(y_3-y_2)\ln(g(y_1))+(y_1-y_3)\ln(g(y_2))+(y_2-y_1)\ln(g(y_3))}\end{cases} \tag{5}$$

3 实验结果分析

为了验证提出的光斑图像中心两步定位算法精度,笔者进行了一系列的仿真测试实验,实验硬件环境为 Core2 处理器,2 GB 内存。

利用 Matlab 分别随机产生 30 幅正常和过度曝光光斑,光斑半径不大于 5,图像大小为 1 024×1 024 且无背景噪声的光斑图像,分别用带阈值的质心法、Hessian 矩阵法和两步定位算法对图像进行处理,计算每幅图像的 RMS 误差,实验结果如图 2 和 3 所示。

由图 2 和图 3 可知,两步定位算法的精度要高于带阈值的质心法和 Hessian 矩阵法。由于正常光斑图像中心不饱和,满足理想高斯分布函数,利用两步定位算法的误差远小于 0.01 像素,而过度曝

光由于中心饱和，其成像模型与理想高斯分布函数有一定的不同，故使用两步定位算法提取和光斑图像中心时的误差有所增加，但仍远小于 0.05 像素。上述实验结果表明,小尺寸光斑中心的两步定位算法满足了高精度的要求，当光斑图像能量分布越接近理想高斯分布时，两步定位算法的精度越高。

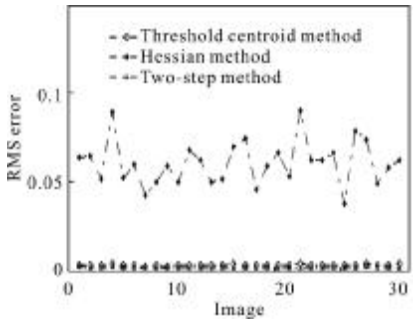

图 2 三种方法对正常光斑图像中心定位的均方根误差

Fig.2 RMS error in center location of normal spot images using three methods

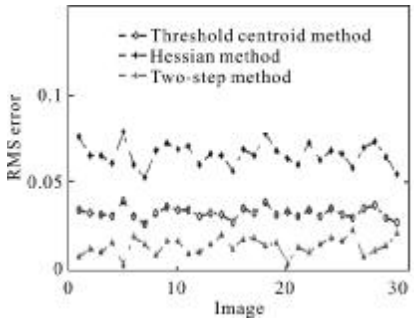

图 3 三种方法对过度曝光光斑图像中心定位的均方根误差

Fig.3 RMS error in center location of over-exposed spot images using three methods

4 结　论

文中提出了一种高精度的小尺寸光斑中心两步定位算法。通过对光斑图像成像模型的分析,通过寻找一阶导数零交叉点的方法准确定位光斑图像像素级中心，再利用高斯拟合方法计算光斑的亚像素级中心点坐标。结果表明,在无噪声情况下,两步定位算法的定位误差在 0.05 像素内,保证了光斑中心的高精度定位,且光斑能量分布越接近理想高斯分布,精度越高。

参考文献:

[1] Lu Z, Liu X, Wang X, et al. High-precision small-scale laser focal spot measurements [J]. High Power Laser and Particle Beams, 2013, 31(1): 177-183. (in Chinese)

[2] Zhang Guangjun. Star Identification [M]. Beijing: National Defense Industry Press, 2011. (in Chinese)

[3] Shortis M, Clarke T, Short T. A comparison of some techniques for the subpixel location of discrete target images [C]//Society of Photo-Optical Instrumentation Engineers, SPIE, 1994, 2287: 239-250.

[4] Steger C. An unbiased detector of curvilinear structures [J]. IEEE Transactions on Pattern Analysis and Machine Intelligence, 1998, 20(2): 113-125.

[5] Wei Zhenzhong, Gao Ming, Zhang Guangjun, et al. Sub-pixel extraction method for the center of light-spot image [J]. Opto-Electronic Engineering, 2009, 36(7): 7-12.

[6] Kong Bing, Wang Zhao, Tan Yushan. Gaussian fitting technique of laser spot [J]. Laser Technology, 2002, 26(4): 277-278. (in Chinese)

[7] Wang Lili, Hu Zhongwen, Ji Hangxin. Laser spot center location algorithm based on Gaussian fitting [J]. Journal of Applied Optics, 2012, 33(5): 985-990. (in Chinese)

[8] Lu Bin, Guo Shaojun, Wang Duo. Centroid Detection of targets on near infrared stellar map based on c spline method and Gauss method comprision [J]. Electro-Optic Technology Application, 2011, 26(5): 59-63. (in Chinese)

[9] Liu Taiyang, Wang Shicheng, Liu Zhiguo, et al. Centroiding algorithm for over-exposed stars based on edge Gaussian interpolation [J]. Opto-Electronic Engineering, 2011, 38(5): 11-15. (in Chinese)

基于曲面拟合的离轴非球面镜顶点半径计算方法

郭玲玲[1,2],任建岳[1],张星祥[1],张立国[1],赵其昌[2],吴泽鹏[2]

(1. 中国科学院长春光学精密机械与物理研究所,吉林 长春 130033;
2. 上海卫星工程研究所,上海 200240)

摘 要:为了解决大口径、离轴非球面顶点半径等参数测量不准的问题,提出了一种基于曲面拟合的非球面参数计算方法。建立了测量坐标系下的非球面准确方程,给出了非线性最小二乘拟合的迭代算法。同时提出了采用补偿器端面数据拟合得到光轴指向,通过测量坐标系下的光轴指向给出合适的拟合初值。对实测数据的实验表明,拟合优度的确定系数接近 1,均方根误差约为 0.002 6 mm,计算结果的顶点半径偏离设计值 0.018 8%。该方法可用于非球面检测阶段的参数计算分析,尤其是计算高精度的顶点半径值,为系统光机装调提供有效的数据支持。

关键词:光学检测; 非球面检测; 顶点半径; 曲面拟合

中图分类号:O439;TH171.65 **文献标志码**:A **文章编号**:1007-2276(2014)08-2694-05

Method to determine vertex radius of off-axis aspheric mirror based on surface fitting

Guo Lingling[1,2], Ren Jianyue[1], Zhang Xingxiang[1], Zhang Liguo[1], Zhao Qichang[2], Wu Zepeng[2]

(1. Changchun Institute of Optics, Fine Mechanics and Physics, Chinese Academy of Sciences, Changchun 130033, China;
2. Shanghai Institute of Satellite Engineering, Shanghai 200240, China)

Abstract: In order to obtain an accurate vertex radius of large-diameter, off-axis aspheric mirrors, a method to determine the geometric parameters of aspheric optical surface based on surface fitting was presented. The accurate aspheric equation under the measuring coordinate system was constructed and an iterative nonlinear least-squares fitting algorithm was given here. Besides, the end surface of the compensator was used to derive the direction of optical axis and then to give appropriate initial values of the surface fitting. The experiments on measured data show that R-square is close to 1 while the root mean square error (RMSE) is about 0.002 6 mm. At the same time, the deviation of the calculated result from the designed value is just 0.018 8% for vertex radius. The method can be utilized to measure and analyze the geometric parameters of aspheric surface-vertex radius for example. It can provide valid data support for the following optical-mechanical assembly.

Key words: optical testing; aspheric measurement; vertex radius; surface fitting

收稿日期:2013-12-05; **修订日期**:2014-01-03

基金项目:国家高技术研究发展计划(863-2-5-1-13B);吉林省科技发展计划(201000526)

作者简介:郭玲玲(1988-),女,硕士生,主要从事空间光学相机测量数据处理及图像处理方面的研究。Email:guolingl@mail.ustc.edu.cn

导师简介:任建岳(1952-),男,研究员,博士生导师,主要从事空间相机光机电一体化设计方面的研究。Email:renjy@ciomp.ac.cn

0 引 言

由于大口径、高精度的离轴非球面光学系统在校正系统像差、提高调制传递函数和分辨率、增大视场、缩小体积重量等方面具有显著优势,故而越来越多地被应用于空间光学遥感器中，典型的如离轴三反系统(TMA)[1-2]。基于大口径离轴非球面的光学系统研究已成为新型高性能空间遥感器发展的重要方向[3]。但是非球面镜自身几何形状的复杂性给加工和检测带来了巨大挑战，尤其是大口径离轴非球面镜的加工和检测难度要远高于球面系统[4-5]。大口径离轴非球面镜参数的测量是非球面检测技术中的关键,也是国内外研究的热点和难点[6-7]。

在 TMA 系统非球面检测中,顶点半径测量的准确性直接决定了系统装调时反射镜之间的相对位置精度,故而需要精确测量[8]。但是,不同于球面系统,大口径离轴非球面镜的顶点半径参数很难直接测量。目前常用的非球面镜面形测量方法为零位补偿干涉法[9-11]。在零位补偿干涉法测量面形达到最好时,可以使用多台经纬仪或一台激光跟踪仪测量非球面上的位置坐标，然后通过曲面拟合的方法得到非球面参数。由于调整误差的存在,直接用准确公式进行拟合时参数较多，难以给出合适的表征旋转误差的参数初值,导致拟合时收敛速度慢甚至不收敛。

文中在零位补偿干涉检测以及激光跟踪仪辅助测量的基础上，提出了使用补偿器端面数据得到光轴指向，从而得到测量坐标系与理论坐标系间的变换关系，解决了使用准确非球面公式进行曲面拟合时收敛性差的问题。并对实测的离轴非球面数据进行了拟合实验，得到了拟合吻合度较高的顶点半径等参数。该方法适用于检测阶段的非球面参数计算分析,从而用于指导系统装调。

1 基于曲面拟合的顶点半径计算模型

1.1 数据拟合模型建立

图 1 所示为使用干涉仪和激光跟踪仪同时测量离轴非球面的示意图,在检测中需要根据非球面的设计参数制造补偿器,通过调整相对位置找到使待测非球面镜达到零条纹干涉,再由激光跟踪仪测量非球面上一组点的坐标。在测量中,补偿器的中轴被调整到与非球面光轴重合,故还可以同时测得补偿器柱面或端面的一组点坐标,从而确定非球面光轴方向。

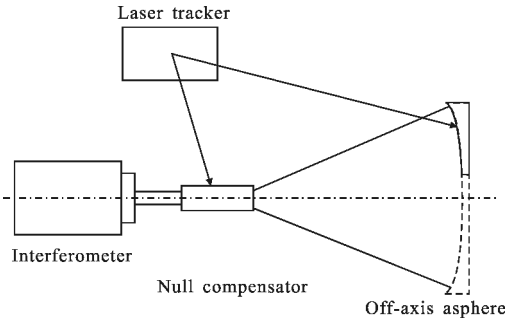

图 1 离轴非球面的检测实验装置

Fig.1 Measuring devices for testing the off-axis asphere

在以虚顶点为原点 **O**，离轴非球面的光轴为 **Z** 轴的理想坐标系下,二次非球面方程为:

$$z=\frac{cr^2}{1+\sqrt{1-(k+1)c^2r^2}} \tag{1}$$

式中:$r^2=x^2+y^2$; 曲率半径 $c=1/R$,R 为顶点半径;k 为圆锥系数。然而实际测量以及所建立的测量坐标系通常与公式(1)所在的理想坐标系存在倾斜及平移,如图 2 所示。

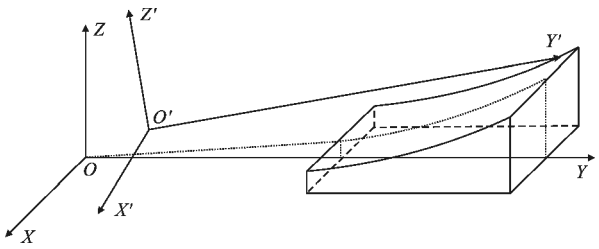

图 2 存在平移、旋转的测量坐标系

Fig.2 Testing coordinates with shift and rotation deviation

在测量坐标系下，如果使用准确非球面公式进行拟合,需要将公式(1)转化到测量坐标系下,即对其进行刚性变换。测量坐标系中坐标$[x',y',z']^T$与理想坐标系中坐标$[x,y,z]^T$关系可以表示为:

$$\begin{bmatrix} x \\ y \\ z \\ 1 \end{bmatrix} = \mathbf{A} \times \begin{bmatrix} x' \\ y' \\ z' \\ 1 \end{bmatrix} \tag{2}$$

式中:×表示矩阵乘操作;变换矩阵 **A** 如公式(3)所示。

由公式(1)~(3)得到测量坐标系下包含旋转和平移参数 α、β、γ、d_1、d_2、d_3 的准确非球面方程为公式(4)所示(为表达清楚,变量符号 x'、y'、z'用 x、y、z 代替)。其中,P_1~P_6 都是无实际意义的中间变量,用于较长公式的表达需要。公式(4)是测量坐标系下的非球面方程显示表达形式,故而可直接用于曲面拟合。公式(4)所示的包含

旋转和平移参数的准确非球面方程可表达三维空间中任何位置的二次非球面，这就使得在非球面检测时位置更随意自由，其缺点在于，由于曲面拟合中代价函数自身的特性，导致了拟合时 α、β、γ 的初值不合适，可能导致拟合不收敛或收敛到的位置为局部最优而非全局最优，故而需要给出合适初值。

$$\mathbf{A}=\begin{bmatrix}1&0&0&\mathbf{d}_1\\0&1&0&\mathbf{d}_2\\0&0&1&\mathbf{d}_3\\0&0&0&1\end{bmatrix}\times\begin{bmatrix}1&0&0&0\\0&\cos\alpha&\sin\alpha&0\\0&-\sin\alpha&\cos\alpha&0\\0&0&0&1\end{bmatrix}\times\begin{bmatrix}\cos\beta&0&\sin\beta&0\\0&1&0&0\\-\sin\beta&0&\cos\beta&0\\0&0&0&1\end{bmatrix}\times\begin{bmatrix}\cos\gamma&\sin\gamma&0&0\\-\sin\gamma&\cos\gamma&0&0\\0&0&1&0\\0&0&0&1\end{bmatrix}=$$
$$\begin{bmatrix}\cos\beta\cos\gamma&\cos\beta\sin\gamma&\sin\beta&\mathbf{d}_1\\-\cos\gamma\sin\alpha\sin\beta-\cos\alpha\sin\gamma&\cos\alpha\cos\gamma-\sin\alpha\sin\beta\sin\gamma&\cos\beta\sin\alpha&\mathbf{d}_2\\-\cos\alpha\cos\gamma\sin\beta+\sin\alpha\sin\gamma&-\sin\alpha\cos\gamma-\cos\alpha\sin\beta\sin\gamma&\cos\beta\cos\alpha&\mathbf{d}_3\\0&0&0&1\end{bmatrix}\tag{3}$$

$$\mathbf{z}=\mathbf{g}(\mathbf{x},\mathbf{y};\mathbf{c},\mathbf{k},\alpha,\beta,\gamma,\mathbf{d}_1,\mathbf{d}_2,\mathbf{d}_3)=\frac{\mathbf{P}_1-\frac{1}{2}\sqrt{\mathbf{P}_2^2-4\mathbf{c}((\mathbf{k}+1)\cos^2\alpha\cos^2\beta+\sin^2\alpha\cos^2\beta+\sin^2\beta)\mathbf{P}_3}}{\mathbf{c}((\mathbf{k}+1)\cos^2\alpha\cos^2\beta+\sin^2\alpha\cos^2\beta+\sin^2\beta)};$$

$$\mathbf{P}_1=\mathbf{cx}\cos\beta\cos\gamma\sin\beta\cos^2\alpha+\mathbf{ckx}\cos\beta\cos\gamma\sin\beta\cos^2\alpha+\mathbf{cy}\cos\beta\sin\beta\sin\gamma\cos^2\alpha+\mathbf{cky}\cos\beta\sin\beta\sin\gamma\cos^2\alpha+\cos\beta\cos\alpha+$$
$$\mathbf{cky}\cos\beta\cos\gamma\sin\alpha\cos\alpha-\mathbf{ckx}\cos\beta\sin\alpha\sin\gamma\cos\alpha-\mathbf{c}\cos\beta\mathbf{d}_3\cos\alpha-\mathbf{ck}\cos\beta\mathbf{d}_3\cos\alpha+\mathbf{cx}\cos\beta\cos\gamma\sin^2\alpha\sin\beta-$$
$$\mathbf{cx}\cos\beta\cos\gamma\sin\beta+\mathbf{cy}\cos\beta\sin^2\alpha\sin\beta\sin\gamma-\mathbf{cy}\cos\beta\sin\beta\sin\gamma-\mathbf{c}\sin\beta\mathbf{d}_1-\mathbf{c}\cos\beta\sin\alpha\mathbf{d}_2;$$
$$\mathbf{P}_2=\mathbf{ck}\cos\beta\sin\beta(\mathbf{x}\cos\gamma+\mathbf{y}\sin\gamma)\cos^2\alpha-2\cos\beta(\mathbf{ckx}\sin\alpha\sin\gamma+\mathbf{c}(\mathbf{k}+1)\mathbf{d}_3-1)\cos\alpha+\mathbf{c}(\cos\beta\mathbf{P}_4-2\sin\beta\mathbf{d}_1);$$
$$\mathbf{P}_3=\mathbf{c}\mathbf{P}_5\cos^2\alpha+2\mathbf{P}_6\cos\alpha+\mathbf{cy}^2\cos^2\gamma\sin^2\alpha+\mathbf{cky}^2\cos^2\gamma\sin^2\alpha+\mathbf{cx}^2\cos^2\gamma\sin^2\alpha\sin^2\beta+\mathbf{cx}^2\sin^2\alpha\sin^2\gamma+\mathbf{ckx}^2\sin^2\alpha\sin^2\gamma+$$
$$\mathbf{cy}^2\sin^2\alpha\sin^2\beta\sin^2\gamma+\mathbf{c}\cos^2\beta(\mathbf{x}\cos\gamma+\mathbf{y}\sin\gamma)^2+\mathbf{cd}_1^2+\mathbf{cd}_2^2+\mathbf{cd}_3^2+\mathbf{ckd}_3^2+2\mathbf{y}\cos\gamma\sin\alpha+\mathbf{ckxy}\cos^2\gamma\sin(2\alpha)\sin\beta-$$
$$2\mathbf{cxy}\cos\gamma\sin^2\alpha\sin\gamma-2\mathbf{ckxy}\cos\gamma\sin^2\alpha\sin\gamma-2\mathbf{x}\sin\alpha\sin\gamma+\mathbf{cxy}\sin^2\alpha\sin^2\beta\sin(2\gamma)+2\mathbf{c}\cos\beta(\mathbf{x}\cos\gamma+\mathbf{y}\sin\gamma)\mathbf{d}_1-$$
$$2\mathbf{cx}\cos\gamma\sin\alpha\cos\beta\mathbf{d}_2-2\mathbf{cy}\sin\alpha\sin\beta\sin\gamma\mathbf{d}_2-2\mathbf{cy}\cos\gamma\sin\alpha\mathbf{d}_3-2\mathbf{cky}\cos\gamma\sin\alpha\mathbf{d}_3+2\mathbf{cx}\sin\alpha\sin\gamma\mathbf{d}_3+2\mathbf{ckx}\sin\alpha\sin\gamma\mathbf{d}_3-2\mathbf{d}_3;$$
$$\mathbf{P}_4=-\mathbf{k}\sin\beta(\mathbf{x}\cos\gamma+\mathbf{y}\sin\gamma)\sin^2\alpha-2\mathbf{d}_2\sin\alpha+\mathbf{k}(\mathbf{y}\cos\gamma\sin(2\alpha)+\mathbf{x}\cos\gamma\sin(\beta)+\mathbf{y}\sin\beta\sin\gamma);$$
$$\mathbf{P}_5=(\mathbf{y}^2+(\mathbf{k}+1)\mathbf{x}^2\sin^2\beta)\cos^2\gamma-2\mathbf{xy}\sin\gamma\cos\gamma+(\mathbf{x}^2+(\mathbf{k}+1)\mathbf{y}^2\sin^2\beta)\sin^2\gamma+(\mathbf{k}+1)\mathbf{xy}\sin^2\beta\sin(2\gamma)$$
$$\mathbf{P}_6=\cos\gamma(\mathbf{cyd}_2+\sin\beta(\mathbf{x}(1-\mathbf{c}(\mathbf{k}+1)\mathbf{d}_3)-\mathbf{ck}(\mathbf{x}^2-\mathbf{y}^2)\sin\alpha\sin\gamma))-\sin\gamma(\mathbf{cxd}_2+\mathbf{y}\sin\beta(\mathbf{ckx}\sin\alpha\sin\gamma+\mathbf{c}(\mathbf{k}+1)\mathbf{d}_3-1))\tag{4}$$

1.2 曲面拟合算法

拟合公式(4)所示的非球面方程，最小二乘测度下的代价函数为未知参数的非线性函数：

$$\mathbf{C}(\vec{t})=\|\mathbf{g}(\mathbf{x}',\mathbf{y}';\vec{t})-\vec{\mathbf{G}}\|^2\tag{5}$$

其中，参数向量 $\vec{t}=[\mathbf{c},\mathbf{k},\alpha,\beta,\gamma,\mathbf{d}_1,\mathbf{d}_2,\mathbf{d}_3]$，$\vec{t}\in\mathbf{R}^8$；$\mathbf{g}(\mathbf{x}',\mathbf{y}';\vec{t})$为测量点处拟合值构成的向量：

$$\mathbf{g}(\mathbf{x}',\mathbf{y}';\vec{t})=[\mathbf{g}(\mathbf{x}_1',\mathbf{y}_1';\vec{t}),\mathbf{g}(\mathbf{x}_2',\mathbf{y}_2';\vec{t}),\cdots,\mathbf{g}(\mathbf{x}_m',\mathbf{y}_m';\vec{t})]^{\mathrm{T}}\tag{6}$$

$\vec{\mathbf{G}}$为测量中获得的 $\mathbf{m}$ 组非球面坐标数据构成的向量：

$$\vec{\mathbf{G}}=[\mathbf{z}_1',\mathbf{z}_2',\cdots,\mathbf{z}_m']^{\mathrm{T}}\tag{7}$$

对于此类非线性最小二乘问题，常用的曲面拟合算法有 Levenberg-Marquardt 法、信赖域(Trust-Region)法。文中采用可以对参数区间进行约束的信赖域法进行拟合，其拟合算法如图 3 所示。

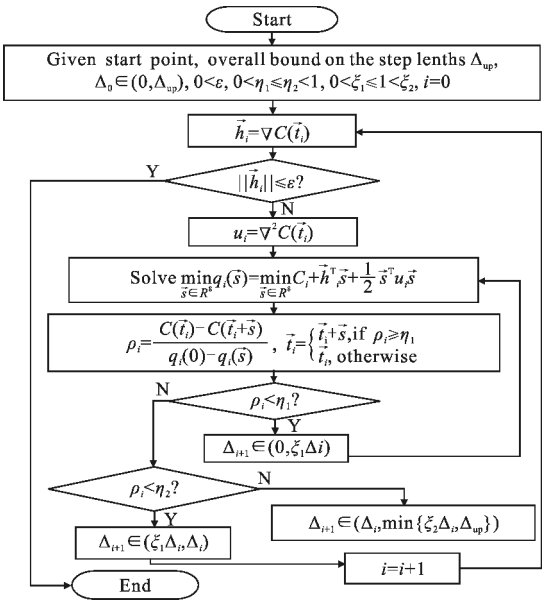

图 3 信赖域拟合曲面方程算法流程

Fig.3 Trust-region algorithm flow of surface fitting

2　基于补偿器端面的初值估算

在第 1 节所介绍的曲面拟合中,α、β、γ 的初值难以确定的一个因素是光轴难以确定,如果已知测量坐标系中的光轴指向,那么就可以通过测量坐标系的光轴指向向量与理论坐标系的光轴指向 $[0,0,1]^{\mathrm{T}}$ 之间的相对位置关系计算得到 α、β、γ。理论上,补偿器端面是与光轴垂直的,故而可以通过补偿器端面上的一组测量点,拟合得到端面方程,其法向即为光轴指向。

2.1　通过补偿器端面测量点拟合光轴指向

补偿器的端面为一平面,其一般方程形式为:

$$z=\mathbf{a}_1x+\mathbf{a}_2y+\mathbf{a}_3 \tag{8}$$

该平面的法向为:

$$\vec{f}'=\begin{bmatrix} -\mathbf{a}_1/\sqrt{\mathbf{a}_1^2+\mathbf{a}_2^2+1} \\ -\mathbf{a}_2/\sqrt{\mathbf{a}_1^2+\mathbf{a}_2^2+1} \\ 1/\sqrt{\mathbf{a}_1^2+\mathbf{a}_2^2+1} \end{bmatrix} \tag{9}$$

通过对测量中得到的端面坐标数据用公式(8)进行曲面拟合即可得到 $\mathbf{a}_1$,$\mathbf{a}_2$,进而得到测量坐标系下的光轴指向 $\vec{f}'$。

2.2　通过光轴指向建立变换关系

在理论坐标系中,光轴指向 $[0,0,1]^{\mathrm{T}}$,故而根据刚性变换理论有公式(10)成立。

$$\begin{bmatrix} 0 \\ 0 \\ 1 \end{bmatrix}=\mathbf{B}\times\vec{f}'=\mathbf{B}\times\begin{bmatrix} -\mathbf{a}_1/\sqrt{\mathbf{a}_1^2+\mathbf{a}_2^2+1} \\ -\mathbf{a}_2/\sqrt{\mathbf{a}_1^2+\mathbf{a}_2^2+1} \\ 1/\sqrt{\mathbf{a}_1^2+\mathbf{a}_2^2+1} \end{bmatrix} \tag{10}$$

式中:$\mathbf{B}$ 为变换矩阵 $\mathbf{A}$ 的左上角 3×3 块矩阵,即

$$\mathbf{B}=\begin{bmatrix} \cos\beta\cos\gamma & \cos\beta\sin\gamma & \sin\beta \\ -\cos\gamma\sin\alpha\sin\beta-\cos\alpha\sin\gamma & \cos\alpha\cos\gamma-\sin\alpha\sin\beta\sin\gamma & \cos\beta\sin\alpha \\ -\cos\alpha\cos\gamma\sin\beta+\sin\alpha\sin\gamma & -\sin\alpha\cos\gamma-\cos\alpha\sin\beta\sin\gamma & \cos\beta\cos\alpha \end{bmatrix} \tag{11}$$

通过公式(10)可以求出 α、β、γ 值,并得到对应的矩阵 $\mathbf{B}$,接下来可以有两种做法,一是直接将求得的 α、β、γ 值作为拟合曲面方程(4)的初值,或者将所测的坐标数据通过矩阵 $\mathbf{B}$ 进行旋转,然后以 0 值作为拟合曲面方程(4)的旋转参数初值。

3　实验与讨论

实验室所测的离轴非球面坐标与补偿器端面坐标在测量坐标系下如图 4 所示,所测非球面含有高次系数,但相较于顶点半径 $\mathbf{R}$ 及二次系数 $\mathbf{k}$,高次系数的绝对值很小($<10^{-17}$),故实验中将其认为是二次非球面进行拟合。由补偿器端面上的测量点所拟合的得到的光轴指向已在图 4 中标识。

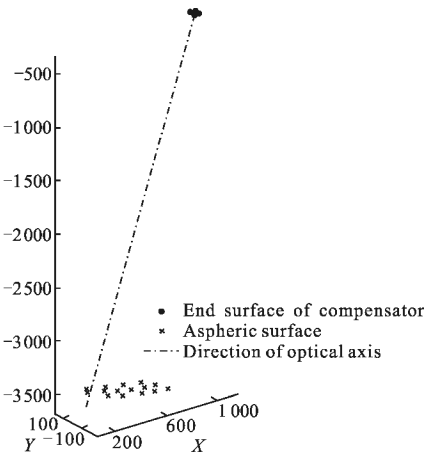

图 4 测量数据及拟合得到的光轴指向

Fig.4 Tested data and fitted direction of optical axis

由测量坐标系下的光轴指向,通过求解公式(10)得到旋转矩阵 $\mathbf{B}$,对非球面测量坐标进行旋转,旋转前后的非球面点对比如图 5 所示。

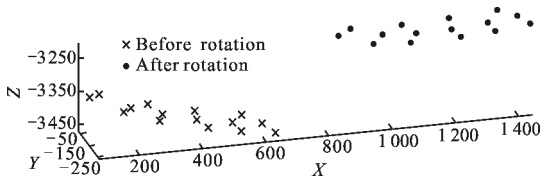

图 5 旋转前后的非球面测量点

Fig.5 Coordinates of tested points before and after rotation

由于旋转并不改变非球面点的相对位置,其作用在于使用公式(4)进行曲面拟合时,α、β、γ 的初值可以给定为 0,保证曲面拟合的收敛速度和收敛结果。对旋转后的测量点使用公式(4)曲面拟合,采用信赖域算法,设置参数向量初始值如下:$[\mathbf{R},\mathbf{k},\alpha,\beta,\gamma,\mathbf{d}_1,\mathbf{d}_2,\mathbf{d}_3]=[3\,200,-0.1,0,0,0,-1\,000,-50,3\,000]$,拟合得到的面形如图 6 所示,参数拟合结果以及拟合优度如表 1 所列。由表 1 结果可知,文中方法得到

的误差平方和 SSE、均方根误差 RMSE 都较小,确定系数 R-square 接近 1,故而拟合吻合度较优。同时顶点半径的测算结果与其设计值的偏差也很小,也在一定程度上说明了该算法计算得到的顶点半径精度较高。除顶点半径外,该方法还得到了圆锥系数 k 的拟合结果,其偏离设计值的百分比稍大,这是由于所测量的非球面实际包含高次系数,忽略高次系数会对 k 的计算结果精度产生一定的影响。

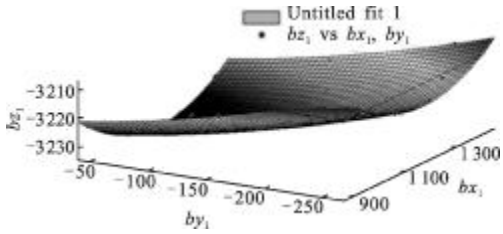

图 6 非球面的曲面拟合

Fig.6 Surface fitting of asphere

表 1 参数拟合结果及拟合优度

Tab.1 Fitting result and goodness

	Fitting results	Deviation from designed values
R/mm	3 220.079 09	0.018 808 80%
k	-0.101 102 188	8.445 723 63%
α/rad	0.001 522 030	-
β/rad	0.013 543 931	-
γ/rad	0.074 906 758	-
d_1/mm	-1 177.838 05	-
d_2/mm	-56.9164072	-
d_3/mm	3 257.432 98	-
SSE/mm^2	0.000 067 72	-
R-square	0.999 999 95	-
RMSE/mm	0.002 602 26	-

4 结 论

通过分析测量坐标系下的非球面准确方程,提出了使用曲面拟合计算顶点半径的方法。在方法实施过程中,采用补偿器端面数据拟合得到光轴指向,从而确定曲面拟合时的初值,解决了曲面拟合过程中不收敛或收敛到的结果非全局最优的问题。通过对实测的离轴非球面坐标数据进行了曲面拟合计算,结果的确定系数十分接近 1,均方根误差约 0.002 6 mm,拟合吻合度较优。该方法可用于非球面检测阶段的参数计算分析,得到较高精度的顶点半径测量结果,从而指导下一步系统装调。

参考文献:

[1] Xue Qingsheng. Design of wide field of view off-axis three-mirror system for hyperspectral imager [J]. Infrared and Laser Engineering, 2012, 41(4): 942-946. (in Chinese)

[2] Guo Jiang, Sun Jiming, Shao Mingdong, et al. Calculation of focal length for off-axis TMA aerospace mapping camera [J]. Optics and Precision Engineering, 2012, 20 (8): 1754-1758. (in Chinese)

[3] Yan Peipei, Fan Xuewu. New design of an off-axis reflective zoom optical system [J]. Infrared and Laser Engineering, 2012, 41(6): 1581-1586. (in Chinese)

[4] Rahman M S, Saleh T, Lim H S, et al. Development of an on-machine profile measurement system in ELID grinding for machining aspheric surface with software compensation [J]. International Journal of Machine Tools & Manufacture, 2008, 48: 887-895.

[5] Li Jie, Wu Fan, Wu Shibin, et al. Determination of measurement point distribution for contact measurement of large aspheric mirror surface [J]. Optics and Precision Engineering, 2012, 20(4): 727-732. (in Chinese)

[6] Xiao M, Jujo S, Takahashi S, et al. Nanometer profile measurement of large aspheric optical surface by scanning deflectometry with rotatable devices: Uncertainty propagation analysis and experiments [J]. Precision Engineering, 2012, 36: 91-96.

[7] Wu Gaofeng, Chen Qiang, Hou Xi, et al. Interferometric testing of vertex radius and conic constant of a conic surface [J]. Acta Optica Sinica, 2009, 29(10): 2804-2807. (in Chinese)

[8] Hu Chunhui, Yan Changxiang. Optical-mechanical assembly based on Gaussian optical homogeneous coordinate transformation [J]. Optics and Precision Engineering, 2012, 20(11): 2353-2359. (in Chinese)

[9] Zhang Jinping, Zhang Xuejun, Zhang Zhongyu, et al. Test of rotationally symmetric aspheric surface using Shack-Hartmann wavefront sensor [J]. Optics and Precision Engineering, 2012, 20(3): 492-498. (in Chinese)

[10] Wyan T J C. Computerized interferometric surface measurements [J]. Applied Optics, 2013, 52(1): 1-8.

[11] Guo Chunfeng, Su Xianyu, Chen Wenjing, et al. Three-dimensional shape measurement of large-aperture aspheric mirrors by off-axis null Ronchi test [J]. Applied Optics, 2012, 51(9): 1276-1282.